nature communications

Article

https://doi.org/10.1038/s41467-025-62566-4

Nucleus-translocated glucokinase functions as a protein kinase to phosphorylate TAZ and promote tumour growth

Received: 27 February 2025

Accepted: 23 July 2025

Published online: 04 August 2025

Check for updates

Gaoxiang Zhao[1,4], Shudi Luo[2,3,4], Hong Zhao[2,3], Qingxia Ma[1], Hongfei Jiang[1], Lin Wang[1], Juanjuan Liu[1], Dong Guo[2,3], Runze Wang[1], Qianqian Xu[1], Jie Lun[1], Ranran Xie[1], Yixin Duan[1], Leina Ma[1], Wensheng Qiu[1] ✉, Jing Fang[1] ✉ & Zhimin Lu[2,3] ✉

Hypoxia frequently occurs during rapid tumour growth. However, how tumour cells adapt to hypoxic stress by remodeling central cellular pathways remains largely unclear. Here, we show that hypoxia induces casein kinase 2 (CK2)-mediated glucokinase (GCK) S398 phosphorylation, which exposes its nuclear localization signal (NLS) for importin α1 binding and nuclear translocation. Importantly, nuclear GCK interacts with the transcriptional coactivator with PDZ-binding motif (TAZ) and functions as a protein kinase that phosphorylates TAZ T346. Phosphorylated TAZ recruits peptidyl-prolyl *cis-trans* isomerase NIMA-interacting 1 (PIN1) for *cis–trans* isomerization of TAZ, which inhibits the binding of β-TrCP to TAZ and β-TrCP-mediated TAZ degradation. Activated TAZ-TEAD induces the expression of downstream target genes to promote tumour growth. These findings reveal an instrumental mechanism by which a glycolytic enzyme regulates the Hippo pathway under hypoxic conditions and highlight the moonlighting function of GCK as a protein kinase in modulating TAZ activity and tumour growth.

Hypoxia, which unavoidably occurs during rapid tumour growth, promotes glycolysis[1]. The first committed step of glycolysis is catalyzed by hexokinase (HK) family members, which convert glucose to glucose-6-phosphate (G-6-P) and are expressed in a tissue-specific manner. Unlike mitochondrion-localized HK1 and HK2, glucokinase (GCK, also known as HK4) is primarily localized in the cytosol and is expressed in the liver, pancreas, small intestine, and brain[2]. Expression of GCK in pancreatic β-cells (pancreatic isoform) and hepatocytes (hepatic isoform) is driven by separate tissue-specific promoters, resulting in two major tissue-specific GCK isoforms that differ only in the first 15 N-terminal amino acids[3]. The glycolytic activity of glycolytic enzymes, including HKs, is critical for aerobic glycolysis and tumour growth[2,4]. However, glycolytic enzymes also exhibit noncanonical or moonlighting functions in response to oncogenic signaling or hypoxic stimulation[5–7]. HK2 under high glucose conditions activates NF-κB pathways to promote tumour immune evasion[7]. Pyruvate kinase muscle isozyme M2 (PKM2) in response to epidermal growth factor receptor (EGFR) activation translocates into the nucleus and activates the β-catenin pathway to enhance tumour cell proliferation[8–12]. However, whether glycolytic enzymes under hypoxic conditions are involved in regulating key cellular signaling pathways to promote tumour growth remains to be elucidated.

The Hippo signaling pathway plays critical roles in regulating many instrumental cellular activities in tumour cells[13–15]. Activation of

[1]Department of Oncology, Cancer Institute of the Affiliated Hospital of Qingdao University, Qingdao University, Qingdao Cancer Institute, Qingdao, Shandong, China. [2]Zhejiang Key Laboratory of Pancreatic Disease, The First Affiliated Hospital, Zhejiang Key Laboratory of Frontier Medical Research on Cancer Metabolism, and Institute of Translational Medicine, Zhejiang University School of Medicine, Hangzhou, Zhejiang, China. [3]Institute of Fundamental and Transdisciplinary Research, Cancer Center, Zhejiang University, Hangzhou, Zhejiang, China. [4]These authors contributed equally: Gaoxiang Zhao, Shudi Luo. ✉e-mail: wsqiuqdfy@qdu.edu.cn; jfang2018@163.com; zhiminlu@zju.edu.cn

this pathway results in phosphorylation of mammalian Ste20-like kinases 1/2 (MST1/2, homologs of Hippo) and activation of large tumour suppressor kinase 1/2 (LATS1/2)[16–18]. LATS1/2 subsequently phosphorylate the transcriptional coactivators TAZ at S89 and YAP at S127, leading to their binding to 14-3-3 and inhibition of their translocation into the nucleus. In addition, LATS1/2 phosphorylates TAZ S311, which primes casein kinase 1 (CK1)-mediated phosphorylation and subsequent β-TrCP-mediated proteasomal degradation[14,19]. When the Hippo pathway is inactive, TAZ and YAP translocate to the nucleus and form a complex with the transcriptional enhanced associate domain (TEAD) transcription factors to promote gene expression and tumour progression[13–15,20–23]. Nevertheless, whether this complex is regulated by the tumour metabolic reprogramming remains largely unclear.

In this report, we demonstrate that hypoxia stimulation induces CK2-mediated GCK phosphorylation at S398 and its subsequent nuclear translocation. Nuclear GCK phosphorylates TAZ at T346, stabilizing TAZ via peptidyl-prolyl *cis-trans* isomerase NIMA-interacting 1 (PIN1)-mediated β-TrCP dissociation from TAZ. Consequently, GCK-induced TAZ-TEAD activation enhances the expression of downstream target genes to promote tumour growth.

Results

GCK S398 phosphorylation by CK2 mediates hypoxia-induced GCK nuclear translocation

HKs respond to extracellular stimuli and exhibit diversified functions[2]. To determine whether hypoxia regulates HKs, we examined the cellular distribution of HKs in MCF7 and BT549 human breast cancer cells under normoxic and hypoxic conditions, using hypoxia-inducible factor (HIF)−1α expression as a responsive and differential marker. Immunofluorescence analyses revealed that hypoxic stimulation induced substantial nuclear translocation of GCK (Fig. 1a) but not HK1 or HK2 (Fig. S1a). The nuclear translocation of GCK was also detected in BT-474 and SK-BR-3 human breast cancer cells by cell fractionation analyses (Figs. 1b and S1b). Analysis of *GCK* mRNA revealed that the pancreatic GCK isoform (1398 nucleotides) is predominantly expressed in breast cancer cells (Fig. S1c). To determine the mechanism underlying the nuclear translocation of GCK, we treated MCF7 cells with a panel of inhibitors, MK-2206, SP600125, SU6656, SB203580, Compound C, GSK2656157, and TBB, which inhibited AKT, c-Jun N-terminal kinase (JNK), c-Src, p38, AMP-activated protein kinase (AMPK), protein kinase R (PKR)-like endoplasmic reticulum kinase (PERK), and casein kinase 2 (CK2), respectively, before hypoxic stimulation (Fig. S1d). The CK2 inhibition, but not others, dramatically blocked hypoxia-induced nuclear translocation of GCK (Fig. 1c). A similar result was also obtained by knockout of CK2α, a catalytic subunit of CK2, using CRISPR-Cas9 genome-editing technology (Fig. 1d). These findings indicate that CK2 activity is required for the nuclear translocation of GCK upon hypoxia stimulation.

Coimmunoprecipitation analyses showed that hypoxia treatment enhanced the binding of HA-GCK, but not HA-HK1 or HA-HK2, to CK2α (Fig. S1e). The CK2α-GCK interaction was also detected in their endogenously expressed proteins (Figs. 1e and S1f). Cell fractionation analyses revealed that this interaction occurred in the cytosol, but not in the nucleus of tumour cells (Fig. S1g). A glutathione S-transferase (GST) pulldown assay showed that purified bacteria-expressed GST-GCK interacted with purified bacteria-expressed His-CK2α (Fig. 1f), indicating that both proteins directly interact with each other.

It was previously shown that ERK activation phosphorylates CK2α at T360/S362, subsequently enhancing CK2α activity[24]. Treatment with the ERK inhibitor U0126 (Fig. S1h), the expression of CK2α T360A/S362A mutant, or treatment the immunoprecipitants with calf intestinal alkaline phosphatase (CIP), which eliminated CK2α T360/S362 phosphorylation (Fig. S1i), abrogated the hypoxia-induced interaction between CK2α and GCK. In addition, the presence of purified active His-ERK2 increased the binding of purified wild-type (WT) GST-CK2α, but not the GST-CK2α T360A/S362A mutant, to His-GCK, and this increase was abolished by CIP treatment (Fig. S1j). These results indicate that hypoxia-induced and ERK-mediated CK2α T360/S362 phosphorylation promotes the binding of CK2 to GCK.

Analyses of the GCK protein sequence using Scansite (http://scansite4.mit.edu/) revealed that GCK S398, which is evolutionarily conserved in different species, is a potential CK2α-phosphorylated residue (Fig. S1k). In vitro phosphorylation analyses showed that purified bacteria-expressed WT GST-CK2α, but not the inactive GST-CK2α K68M mutant, phosphorylated purified WT His-GCK but not His-GCK S398A (Fig. 1g). This phosphorylation was also detected using a specificity-validated anti-GCK pS398 antibody (Figs. 1g and S1l, m). Consistently, hypoxia treatment of MCF7 cells induced the phosphorylation of GCK S398 in breast cancer cells expressing WT GCK but not in those expressing the GCK S398A mutant (Fig. 1h). In addition, this phosphorylation in MCF7 (Fig. 1i), BT-474, and SK-BR-3 cells (Fig. S1n) was abolished by TBB treatment. Notably, the GCK S398A mutant failed to translocate into the nucleus in MCF7 and BT549 cells upon hypoxia stimulation (Fig. 1j, k), whereas the phosphorylation-mimicking GCK S398D mutant translocated into the nucleus under normoxic conditions (Fig. 1j, k). In addition, neither GCK S398A nor GCK S398D affected glucose uptake or lactate production in MCF7 cells under hypoxic conditions (Fig. S1o), which is likely attributed to the unaltered distribution of highly activated HK1/2. These results indicate that GCK S398 phosphorylation by CK2 mediates hypoxia-induced nuclear translocation of GCK.

GCK binds to importin α1 for nuclear translocation

Importin α family proteins (α1, α3, α4, α5, α6, and α7) regulate protein nuclear translocation[25]. A Streptavidin agarose pulldown assay showed that S-protein-Flag-streptavidin binding peptide (SFB)-tagged importin α1, but not importin α3, α4, α5, α6, or α7, bound to HA-GCK expressed in breast cancer cells (Fig. S2a). This interaction was also detected between endogenous GCK and endogenous importin α1 in MCF7 cells (Fig. 2a). In addition, depletion of importin α1 via the expression of *KPNA2* (encoding importin α1) short hairpin RNA (shRNA) markedly blocked hypoxia- or CK2α overexpression-induced nuclear translocation of GCK (Figs. 2b and S2b), revealing the essential role of importin α1 in the nuclear translocation of GCK.

Importin α functions as an adaptor that links nuclear localization signal (NLS)-containing proteins with importin α, which then docks the ternary complex at the nuclear pore complex to facilitate translocation of these proteins across the nuclear envelope[10]. Analyses of the protein sequence of GCK revealed that residues 341-373 may contain an NLS, which is evolutionarily conserved across different species (Fig. S2c). An in vitro GST pull-down assay showed that purified GST-importin α1 failed to interact with the purified His-GCK NLS mutant (R368A/R369A) or His-GCK S398A (Fig. S2d). Consistently, GCK R368A/R369A or GCK S398A, unlike its WT counterpart, was unable to bind to endogenous importin α1 in MCF7 cells upon hypoxic stimulation (Fig. 2c), suggesting that GCK S398 phosphorylation exposes its NLS for importin α1 binding. This finding was substantiated by molecular dynamics simulation analyses, which showed that GCK S398 phosphorylation by CK2α promoted the outward flipping of R368 in the NLS (Fig. S2e), likely facilitating the binding of importin α1 to the GCK NLS and promoting GCK's nuclear translocation.

Coimmunoprecipitation analyses showed that HA-importin α1 interacted with Flag-GCK S398D, but not Flag-GCK S398A, under normoxic conditions (Fig. S2f). Notably, the GCK R368A/R369A mutation abolished the nuclear translocation of both WT GCK under hypoxic conditions (Fig. 2d, e) and Flag-GCK S398D under normoxic conditions (Fig. S2g, h) in both MCF7 and BT549 cells, as detected by cell fractionation (Figs. 2d and S2g) and immunofluorescence (Figs. 2e and S2h) analyses. These results indicate that phosphorylation of GCK

https://doi.org/10.1038/s41467-025-62566-4

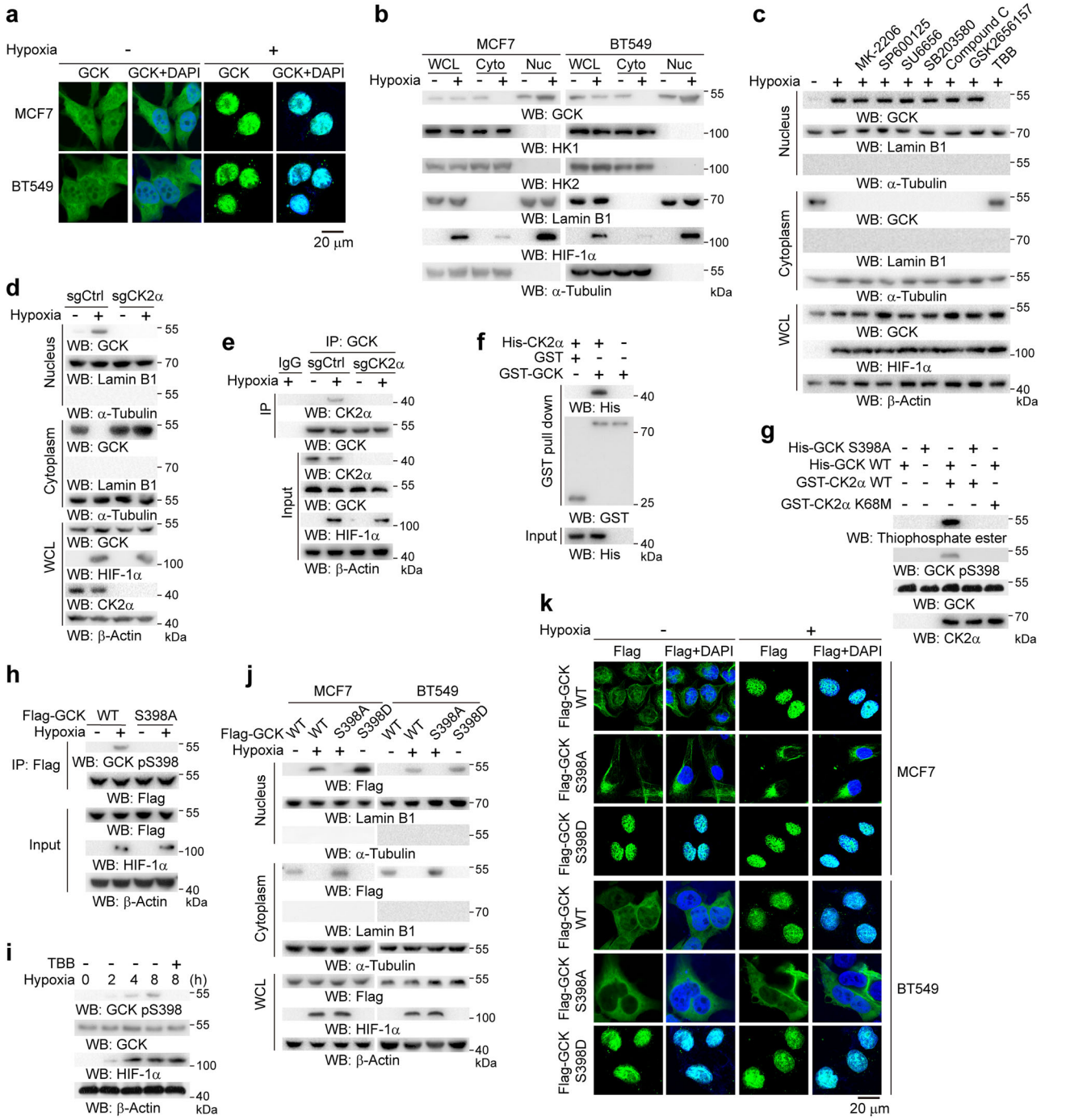

Fig. 1 | GCK S398 phosphorylation by CK2 induces nuclear translocation of GCK. a MCF7 and BT549 cells were stimulated with or without hypoxia for 8 h. Immunofluorescence analyses were performed with an anti-GCK antibody. DAPI (blue) was used to stain the nuclei. **b** MCF7 (luminal A) and BT549 (basal) cells were treated with or without hypoxia for 8 h. Whole-cell lysates (WCLs) were collected and cytosolic (Cyto) and nuclear (Nuc) fractions were prepared. WB, western blot. **c** MCF7 cells were pretreated with or without the indicated inhibitors for 30 min and then treated with or without hypoxia and the indicated inhibitors for 8 h. Cytoplasm and nucleus were prepared. Whole-cell lysates were collected. **d** MCF7 cells with or without CK2α knockout were subjected to hypoxia for 8 h. Cytoplasm and nucleus were prepared. WCLs were collected. **e** MCF7 cells with or without CK2α knockout were subjected to hypoxia for 8 h. Immunoprecipitation (IP) with an anti-GCK antibody was performed. **f** A GST pulldown assay was performed by mixing purified His-CK2α with purified GST or GST-GCK. Immunoblotting analyses were performed as indicated. **g** An in vitro kinase assay was performed by incubating GST-CK2α WT or GST-CK2α K68M with His-GCK WT or His-GCK S398A in the presence of active ERK2 and ATP-γ-S. The samples were then alkylated with p-nitrophenyl mesylate (PNBM). **h** MCF7 cells expressing Flag-GCK WT or Flag-GCK S398A were treated with or without hypoxia for 8 h. IP analyses were performed with an anti-Flag antibody. **i** MCF7 cells pretreated with or without TBB (10 μM) for 30 min were subjected to hypoxia or/and TBB for the indicated times. Total cell lysates were prepared. **j** MCF7 and BT549 cells transfected with the indicated plasmids were treated with or without hypoxia for 8 h. Cytoplasm and nucleus were prepared. WCL was collected. **k** MCF7 and BT549 cells transfected with the indicated plasmids were stimulated with or without hypoxia for 8 h. Immunofluorescence analyses were performed with an anti-Flag antibody. DAPI (blue) was used to stain the nuclei. All immunoblotting and immunofluorescence experiments were performed in at least three independent biological replicates, with consistent results observed across repetitions. Representative data are shown. Source data are provided as a Source Data file.

https://doi.org/10.1038/s41467-025-62566-4

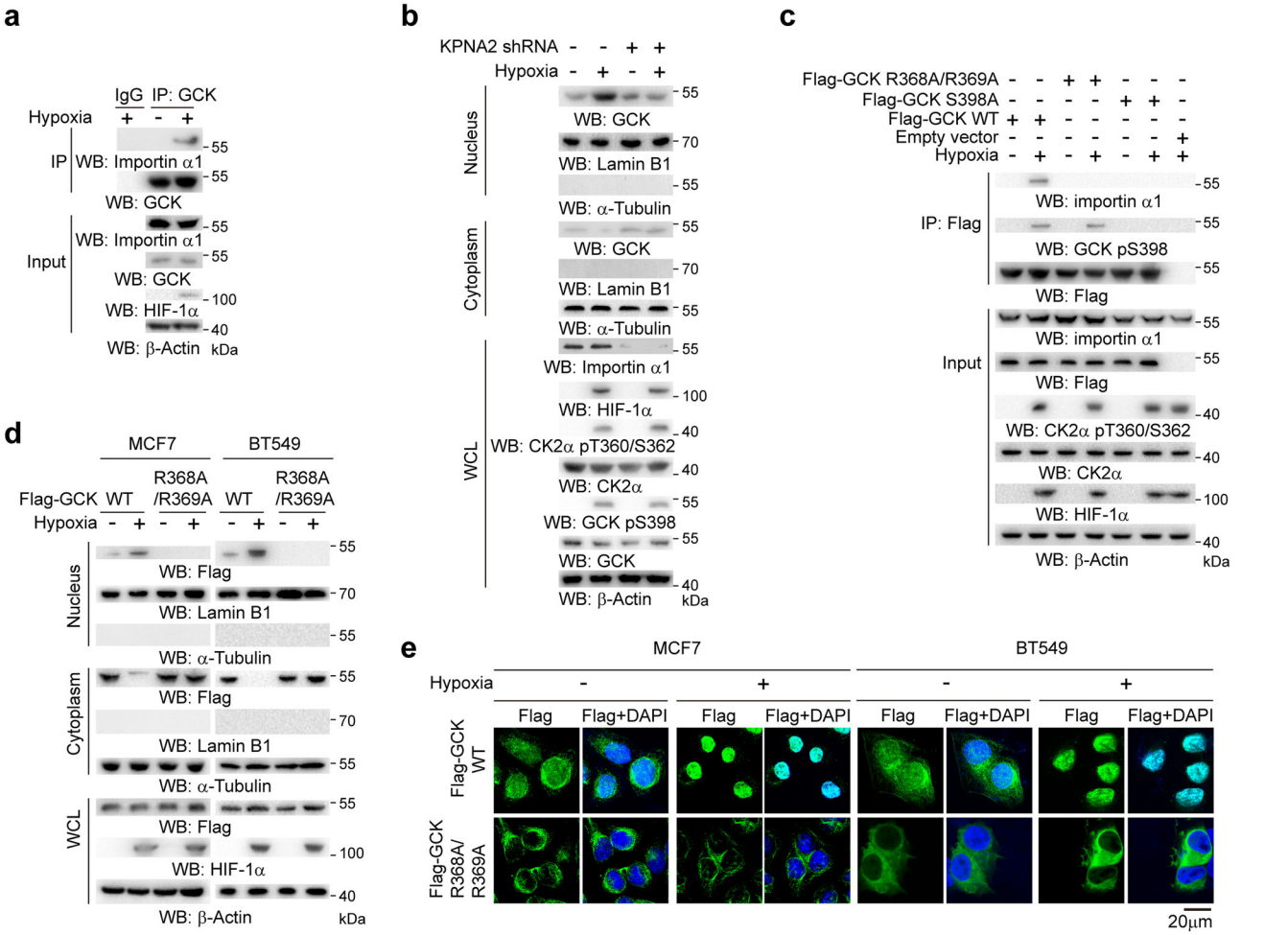

Fig. 2 | GCK binds to importin α1 for nuclear translocation. a MCF7 cells were treated with or without hypoxia for 8 h. Immunoprecipitation with an anti-GCK antibody was performed. **b** MCF7 cells with or without importin α1 (encoded by *KPNA2*) depletion were treated with or without hypoxia for 8 h. WCL and cytoplasm and nucleus were prepared. **c** MCF7 cells expressing the indicated Flag-GCK proteins were treated with or without hypoxia for 8 h. IP with an anti-Flag antibody was performed. **d** MCF7 and BT549 cells expressing the indicated Flag-GCK proteins were treated with or without hypoxia for 8 h. WCL and cytoplasm and nucleus were prepared. **e** The indicated Flag-GCK proteins were expressed in MCF7 and BT549 cells. Immunofluorescence analyses were performed with an anti-Flag antibody. DAPI (blue) was used to stain the nuclei. All immunoblotting and immunofluorescence experiments were performed in at least three independent biological replicates, with consistent results observed across repetitions. Representative data are shown. Source data are provided as a Source Data file.

S398 by CK2 enables R368/R369 in the NLS of GCK to bind to importin α1, leading to subsequent nuclear translocation of GCK.

Nuclear GCK functions as a protein kinase and phosphorylates TAZ at T346

To determine the nuclear function of GCK, we performed mass spectrometry analyses of GCK S398D immunoprecipitants from hypoxia-stimulated MCF7 cells and revealed that GCK interacted with the transcriptional coactivator TAZ (Fig. S3a and Supplementary Data 2). This interaction was validated by coimmunoprecipitation analyses (Fig. S3b), which also showed that hypoxia stimulation induced the binding of endogenous GCK to endogenous TAZ in the nucleus, but not in the cytosol, of MCF7 cells (Fig. 3a). In contrast, purified GST-GCK S398D did not bind to purified YAP in vitro (Fig. S3c). It is known that 14-3-3 binds to and sequesters S89-phosphorylated TAZ by LATS1/2 in the cytosol and that unphosphorylated TAZ accumulates in the nucleus[14,26]. As expected, purified 14-3-3 blocked the binding of purified GST-GCK WT to the purified His-TAZ S89D phosphorylation-mimicking mutant (Fig. 3b). In contrast, 14-3-3 failed to disrupt the interaction between the GST-GCK S398D phosphorylation-mimicking mutant and WT His-TAZ (Fig. 3b), further supporting that S398-phosphorylated GCK binds to activated TAZ in the nucleus.

Given that metabolic enzymes can function as protein kinases[8,27,28], we performed an in vitro protein phosphorylation assay by incubating purified GST-GCK S398D with purified His-TAZ WT. Liquid chromatography-tandem mass spectrometry (LC–MS/MS) analyses showed that TAZ was phosphorylated at the evolutionarily conserved T346 residue (Fig. S3d, e), which is located in the transcriptional activation domain (Fig. S3f)[13–15]. This in vitro phosphorylation, which was also detected using a specificity-validated anti-TAZ pT346 antibody, was abolished by the TAZ T346A mutation (Figs. 3c and S3g, h). This mutation also inhibited hypoxia-induced or GCK S398D-dependent TAZ T346 phosphorylation (Fig. 3d) without affecting LATS1/2-mediated phosphorylation of TAZ at S89 or S311 (Fig. S3i). These results suggest that TAZ is regulated by LATS1/2-mediated cytosolic TAZ S89/S311 phosphorylation and GCK-mediated nuclear TAZ T346 phosphorylation.

We next used CRISPR-Cas9 genome-editing technology and created knock-in expression of TAZ T346A in both MCF7 and BT549 cells (Fig. S3j–l). Consistently, the knock-in expression of TAZ T346A (Fig. 3e), as well as GCK knockout (Fig. 3f), abrogated hypoxia-induced TAZ T346 phosphorylation in breast cancer cells. These results indicate that nuclear GCK functions as a protein kinase and phosphorylates TAZ at T346.

https://doi.org/10.1038/s41467-025-62566-4

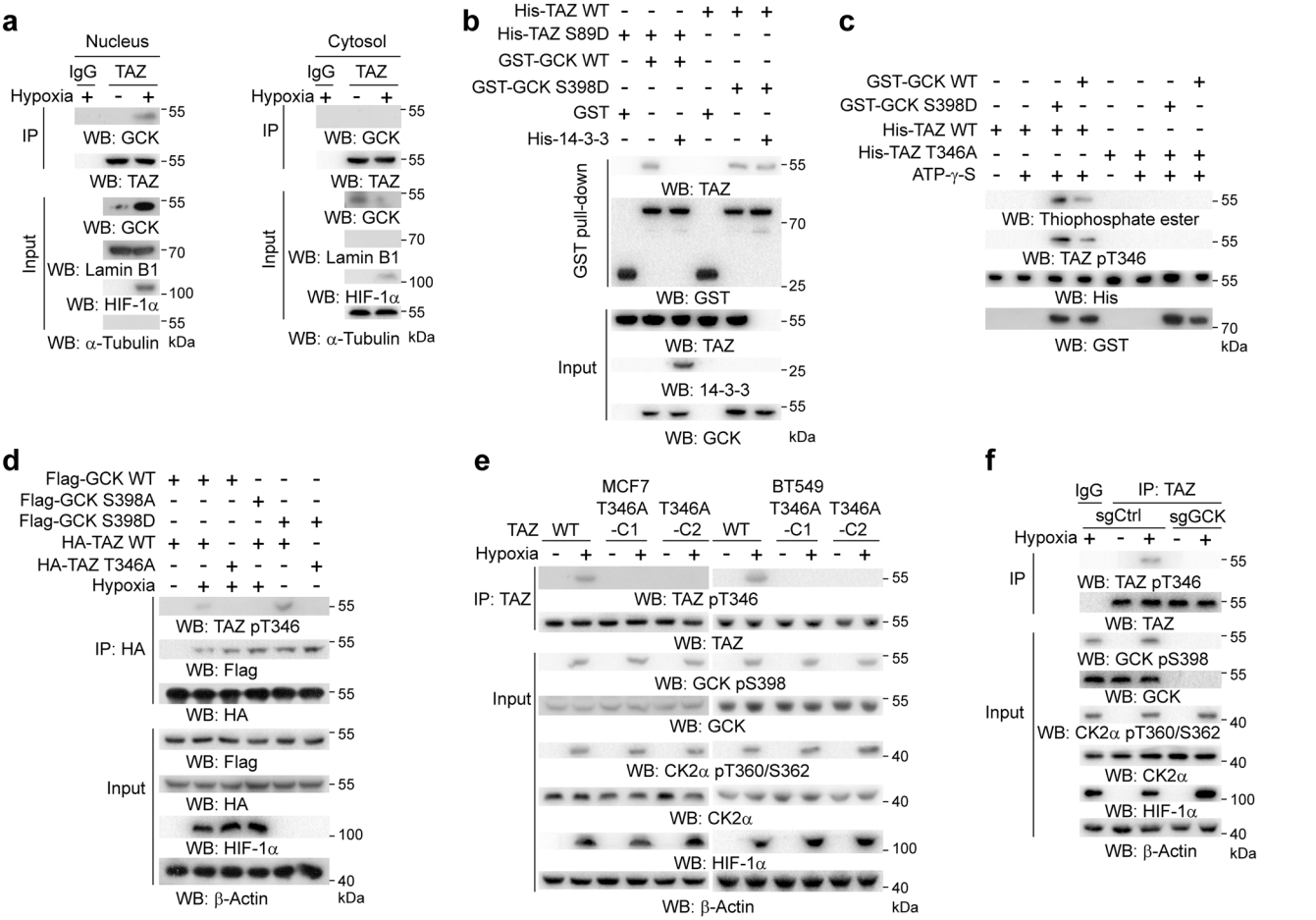

Fig. 3 | Nucleus-translocated GCK acts as a protein kinase to phosphorylate TAZ. a MCF7 cells were treated with or without hypoxia for 8 h. Cytosolic and nuclear fractions were prepared. IP with an anti-TAZ antibody was performed. **b** A GST pull-down assay was performed by mixing purified His-TAZ protein with purified GST or GST-GCK in the presence or absence of purified 14-3-3. **c** An in vitro kinase assay was performed by mixing GST-GCK WT/S398D with His-TAZ WT/T346A proteins in the presence of ATP-γ-S. The samples were then alkylated with PNBM. **d** MCF7 cells transfected with the indicated plasmids were treated with or without hypoxia for 8 h, after which IP and WB analyses were performed with the indicated antibodies. **e** Parental MCF7 and BT549 cells and the indicated clones with knocked-in expression of TAZ T346A were stimulated with or without hypoxia for 8 h. IP with an anti-TAZ antibody was performed. **f** MCF7 cells with or without GCK knockout were treated with or without hypoxia for 8 h. IP with an anti-TAZ antibody was performed. All immunoblotting and immunofluorescence experiments were performed in at least three independent biological replicates, with consistent results observed across repetitions. Representative data are shown. Source data are provided as a Source Data file.

Nuclear GCK-mediated TAZ phosphorylation recruits PIN1 and increases TAZ stability and transcriptional activity

A time-course experiment showed that hypoxic stimulation increased TAZ T346 phosphorylation, which was correlated with upregulated TAZ expression (Fig. 4a). Knock-in expression of TAZ T346A markedly decreased TAZ expression in both MCF7 and BT549 cells (Fig. 4b). Consistently, compared with GCK S398A, GCK S398D increased the half-life of both WT TAZ (Fig. 4c) and the mutants TAZ S89A and S311A (Fig. S4a) in breast cancer cells in the presence of cycloheximide (CHX), a protein translation inhibitor. These results indicate that nuclear GCK increases TAZ stability independent of LATS1/2-mediated cytosolic TAZ S89/S311 phosphorylation.

Consistently, knock-in expression of GCK S398D in both MCF7 and BT549 cells (Fig. S4b–d) increased TAZ stability (Fig. 4d) without obviously altering the mRNA level of *WWTR1* (encoding TAZ) (Fig. S4e). In addition, hypoxic stimulation had little effect on *WWTR1* mRNA expression (Fig. S4f), indicating that hypoxia-induced and CK2α-mediated GCK S398 phosphorylation increases TAZ stability independent of its gene transcription. Consistent with these findings, TAZ T346A had a much shorter half-life than phosphorylation-mimicking TAZ T346E in breast cancer cells (Fig. S4g). These results indicate that nuclear GCK-mediated TAZ T346 phosphorylation increases TAZ stability.

Analysis of the TAZ protein sequence revealed that T346 is followed by a proline. It is known that phosphorylated pS/TP peptide sequences can be recognized and *cis-trans* isomerized by the peptidyl-proline isomerase protein never in mitosis gene A interacting-1 (PIN1)[29]. Upon hypoxic stimulation, endogenous PIN1 bound to endogenous TAZ (Fig. 4e), and this interaction, as well as the hypoxia-induced increase in TAZ expression (Fig. 4e), was blocked by CK2α depletion. Additionally, the expression of a substrate-binding-deficient Flag-PIN1 WW domain mutant (WWm) or TAZ T346A inhibited hypoxia-induced the PIN1-TAZ interaction, whereas TAZ T346E was able to bind to PIN1 without hypoxia stimulation (Fig. 4f). Consistently, a GST pulldown assay showed that purified WT His-TAZ bound to purified WT GST-PIN1, but not to the GST-PIN1 WW mutant, only in the presence of GCK S398D and ATP (Fig. 4g).

To further determine whether the phosphorylated T346/P347 motif of TAZ is a PIN1 substrate, we synthesized oligopeptides of TAZ containing phosphorylated or nonphosphorylated T346/P347. As expected, WT GST-PIN1 isomerized the phosphorylated T346/P347 peptide much more efficiently than did a catalytically inactive GST-

https://doi.org/10.1038/s41467-025-62566-4

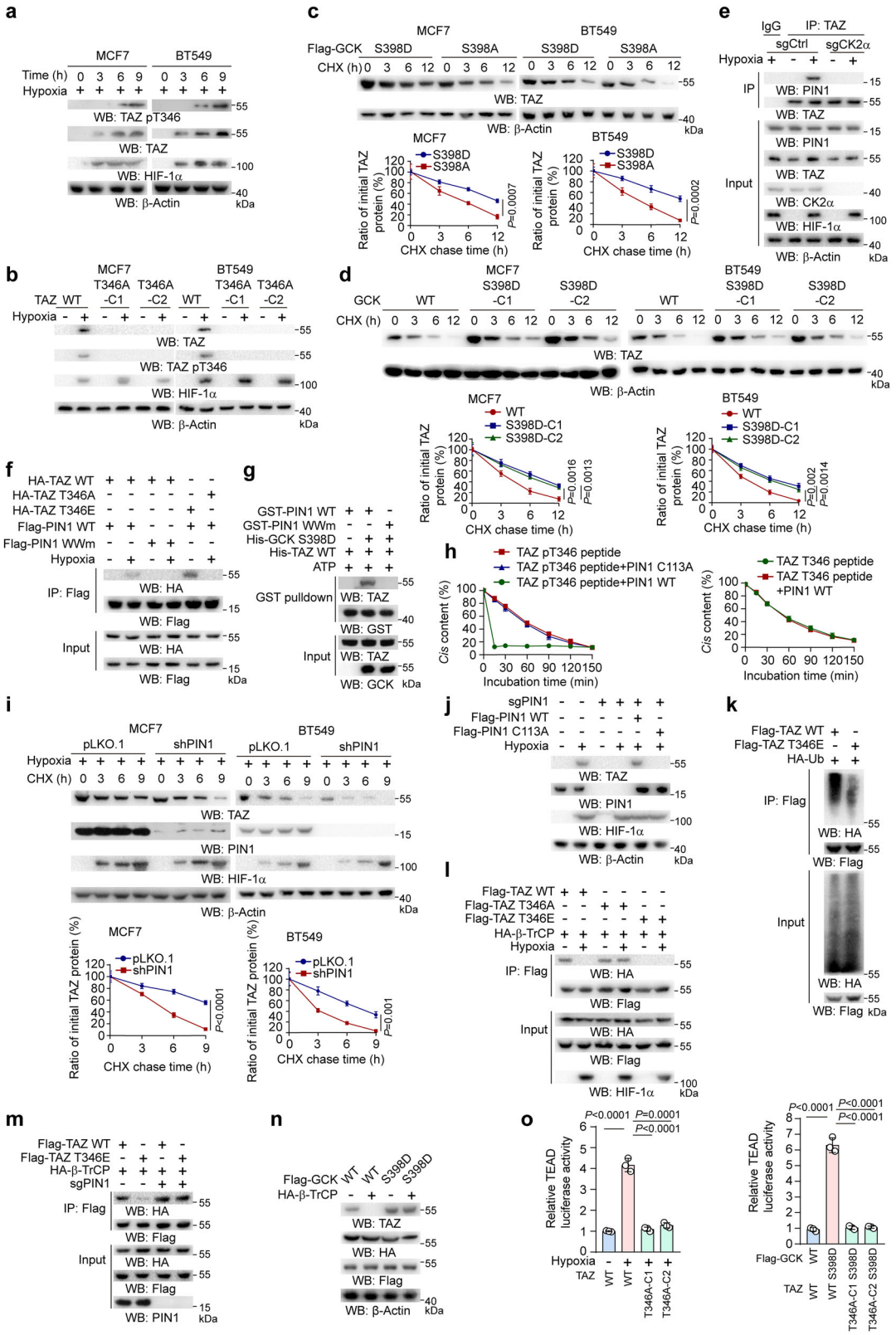

PIN1 C113A mutant (Fig. 4h, left panel), whereas WT PIN1 failed to isomerize the nonphosphorylated counterpart (Fig. 4h, right panel), suggesting that PIN1 specifically isomerizes the phosphorylated T346/P347 within TAZ. Notably, the depletion of PIN1 in MCF7 cells shortened the half-life of TAZ in CHX-treated MCF7 and BT549 cells (Fig. 4i). In addition, PIN1 deficiency blocked hypoxia-induced TAZ expression, and this block was eliminated by reconstituted expression of WT PIN1 but not by PIN1 C113A (Fig. 4j). These results indicate that nuclear GCK-mediated TAZ phosphorylation recruits PIN1 to TAZ, leading to the *cis-trans* isomerization and subsequent stabilization of TAZ.

To further explore the mechanism underlying GCK-mediated TAZ stabilization, we expressed HA-Ub and showed that compared with its WT counterpart, TAZ T346E exhibited reduced TAZ polyubiquitination

Fig. 4 | Nuclear GCK-mediated TAZ phosphorylation recruits PIN1 and increases TAZ stability and transcriptional activity. a The indicated cells were subjected to hypoxia for the indicated periods. WB analyses with the indicated antibodies were performed. **b** Parental MCF7 and BT549 cells and the indicated clones with knock-in expression of TAZ T346A mutants were stimulated with or without hypoxia for 8 h. WB analyses were performed with the indicated antibodies. **c**, **d** MCF7 and BT549 cells were transfected with the indicated plasmids (**c**). The indicated clones of these cells with knock-in expression of GCK S398D were constructed (**d**). These cells were treated with 100 μg/mL cycloheximide (CHX) prior to WB analysis. The quantification of TAZ protein levels relative to initial protein levels is shown. The data are the means ± SD, n = 3 independent experiments, by two-tailed Student's t tests (**c**, **d**). **e** MCF7 cells with or without CK2α knockout were treated with or without hypoxia for 8 h. IP and WB analyses were performed with the indicated antibodies. **f** MCF7 cells transfected with the indicated plasmids were treated with or without hypoxia for 8 h before IP and WB analyses. **g** Purified GST-PIN1 WT or GST-PIN1 WW mutant was mixed with the indicated purified His-TAZ proteins in the presence or absence of purified His-GCK S398D and ATP. A GST pull-down assay was subsequently performed. **h** *Cis–trans* isomerization assays were carried out by mixing synthesized phosphorylated or nonphosphorylated oligopeptide of TAZ containing the T346P motif with purified WT GST-PIN1 or GST-PIN1 C113A mutant. Data represent the means ± SD of three independent experiments. **i** MCF7 and BT549 cells with or without PIN1 shRNA expression were treated with CHX (100 μg/mL) and harvested at the indicated times. WB analyses were performed with the indicated antibodies. The quantification of TAZ protein levels relative to initial protein levels is shown. The data are the means ± SD, n = 3 independent experiments, by two-tailed Student's t tests. **j** MCF7 cells transfected with the indicated plasmids were treated with or without hypoxia for 8 h before WB analysis. **k** MCF7 cells transfected with the indicated plasmids were treated with 10 μM MG132 for 10 h before IP and WB analyses. **l** MCF7 cells transfected with the indicated plasmids were treated with or without hypoxia for 8 h before IP and WB analyses. **m** MCF7 cells were transfected with the indicated plasmids. IP and WB analyses were then performed. **n** MCF7 cells were transfected with the indicated plasmids. WB analyses were then performed. **o** Parental MCF7 and BT549 cells and the indicated clones with knock-in expression of TAZ T346A mutant stably expressing a luciferase reporter, which was driven by the CTGF promoter, were stimulated with or without hypoxia for 8 h or transfected with the indicated plasmids. A luciferase reporter assay was then performed. The data are the means ± SD, n = 3 independent experiments, by two-tailed Student's t tests. All immunoblotting and immunofluorescence experiments were performed in at least three independent biological replicates, with consistent results observed across repetitions. Representative data are shown. Source data are provided as a Source Data file.

(Fig. 4k). Since TAZ is known to bind to β-TrCP and is degraded by the E3 ligase Cullin1-β-TrCP[19], we performed coimmunoprecipitation analyses and showed that hypoxia induced the disassociation of β-TrCP from WT TAZ but not TAZ T346A (Fig. 4l). In contrast, TAZ T346E lost its ability to bind to β-TrCP in the absence of hypoxic stimulation, and this deficiency was rescued by PIN1 depletion (Fig. 4m). As expected, β-TrCP overexpression decreased TAZ expression but did not affect GCK S398D-mediated upregulation of TAZ expression (Fig. 4n). These results indicate that GCK-mediated TAZ phosphorylation and subsequent PIN1-mediated *cis-trans* isomerization inhibit β-TrCP-dependent TAZ polyubiquitination and degradation.

Nuclear TAZ binds to and activates TEAD transcription factors[30]. As expected, hypoxia stimulation (Figs. 4o and S4h) or GCK S398D expression (Figs. 4o and S4i) dramatically increased TEAD activity, as detected by a luciferase reporter assay (Fig. 4o) and the expression of the TAZ-TEAD target genes, such as connective tissue growth factor (*CTGF*), Cysteine-rich angiogenic inducer 61 (*CYR61*), AXL receptor tyrosine kinase (*AXL*), and caudal type homeobox 2 (*CDX2*), in different breast cancer cells (Fig. S4h, i). This upregulation was diminished in cells with knock-in expression of TAZ T346A (Figs. 4o and S4h, i), suggesting that GCK-mediated TAZ phosphorylation enhances TEAD transcriptional activity and downstream gene expression. Together, these results indicate that nuclear GCK-mediated TAZ phosphorylation recruits PIN1 and increases TAZ stability and transcriptional activity.

Nuclear GCK-mediated TAZ phosphorylation and activation promotes tumour cell proliferation and tumour growth

Consistent with GCK-promoted TAZ-TEAD transcriptional activity, GCK S398D expression markedly enhanced the proliferation (Fig. 5a), colony formation (Fig. 5b), and migration (Fig. S5a) of both MCF7 and BT549 cells. This enhancement was abrogated by knock-in expression of TAZ T346A (Figs. 5a, b and S5a), which also inhibited hypoxia- or CK2α overexpression-enhanced colony formation (Fig. S5b, c). In contrast, knock-in expression of TAZ T346E (Fig. S5d–f) or GCK S398D in MCF7 and BT549 cells increased colony formation (Fig. S5g, h). Notably, GCK S398D-enhanced colony formation was abrogated by TAZ depletion (Fig. S5h), revealing a dependency of nuclear GCK-induced cell proliferation on TAZ expression. These results indicate that nuclear GCK-mediated TAZ phosphorylation promotes the proliferation and migration of breast cancer cells.

We next orthotopically injected MCF7 cells with or without knock-in expression of GCK S398D or GCK S398A (Fig. S5i–k) into the fourth mammary fat pad of athymic nude mice. Compared with WT GCK expression, GCK S398D expression markedly increased tumour growth (Fig. 5c, d), while GCK S398A expression reduced tumour growth (Fig. 5c, d). Immunohistochemistry (IHC) analyses of the tumour tissue revealed that GCK S398D expression increased TAZ T346 phosphorylation and expression of TAZ and CTGF (Fig. 5e), whereas the opposite results were observed in tumour tissues expressing GCK S398A (Fig. 5e). In addition, knock-in expression of TAZ T346E or TAZ T346A mirrored the effects of GCK S398D or GCK S398A, respectively (Fig. 5f–h). Notably, knock-in expression of TAZ T346A mitigated GCK S398D-promoted tumour growth (Fig. 5i, j), TAZ T346 phosphorylation, and expression of TAZ and CTGF (Fig. 5k). Of note, immunofluorescent analysis of tumour tissues showed that the levels of HIF-1α (Fig. S5l) or CK2α T360/S362 phosphorylation (Fig. S5m) correlated with the phosphorylation levels of GCK S398 and TAZ T346, suggesting that hypoxia regulates the phosphorylation of GCK S398 by CK2 and TAZ T346 by GCK. These results indicate that nuclear GCK-mediated TAZ phosphorylation and stabilization promotes tumour growth by enhancing TAZ-TEAD transcriptional activity.

Discussion

Compared with normal cells, tumour cells exhibit enhanced anti-stress plasticity, granting them a selective advantage for survival and proliferation under challenging microenvironmental conditions, such as hypoxia. Nevertheless, the precise mechanisms by which tumour cells modulate gene expression to promote tumour cell proliferation in response to hypoxic stress remain to be fully elucidated. We demonstrated that hypoxia stimulation of tumour cells leads to CK2-mediated phosphorylation of GCK at S398, facilitating the exposure of the NLS of GCK. This exposed NLS enables the recognition of GCK by importin α1, promoting its subsequent nuclear translocation. In the nucleus, GCK forms complexes with TAZ, serving as a protein kinase that phosphorylates TAZ at T346. This phosphorylation leads to the recruitment of PIN1, leading to the *cis-trans* isomerization and subsequent stabilization of TAZ through its dissociation from β-TrCP. This stabilization, in turn, promotes TAZ-TEAD activation, the expression of their downstream genes, including *CTGF, CYR61, AXL* and *CDX2*, proliferation of breast cancer cells, and breast tumour growth in mice. These findings underscore the critical role of nuclear GCK-mediated TAZ T346 phosphorylation and stabilization in tumour growth (Fig. 6). Given that protein kinases can phosphorylate multiple protein substrates, the finding that GCK possesses protein kinase activity implies that it may phosphorylate different protein substrates, thereby regulating their functions in response to distinct upstream signalings[31].

https://doi.org/10.1038/s41467-025-62566-4

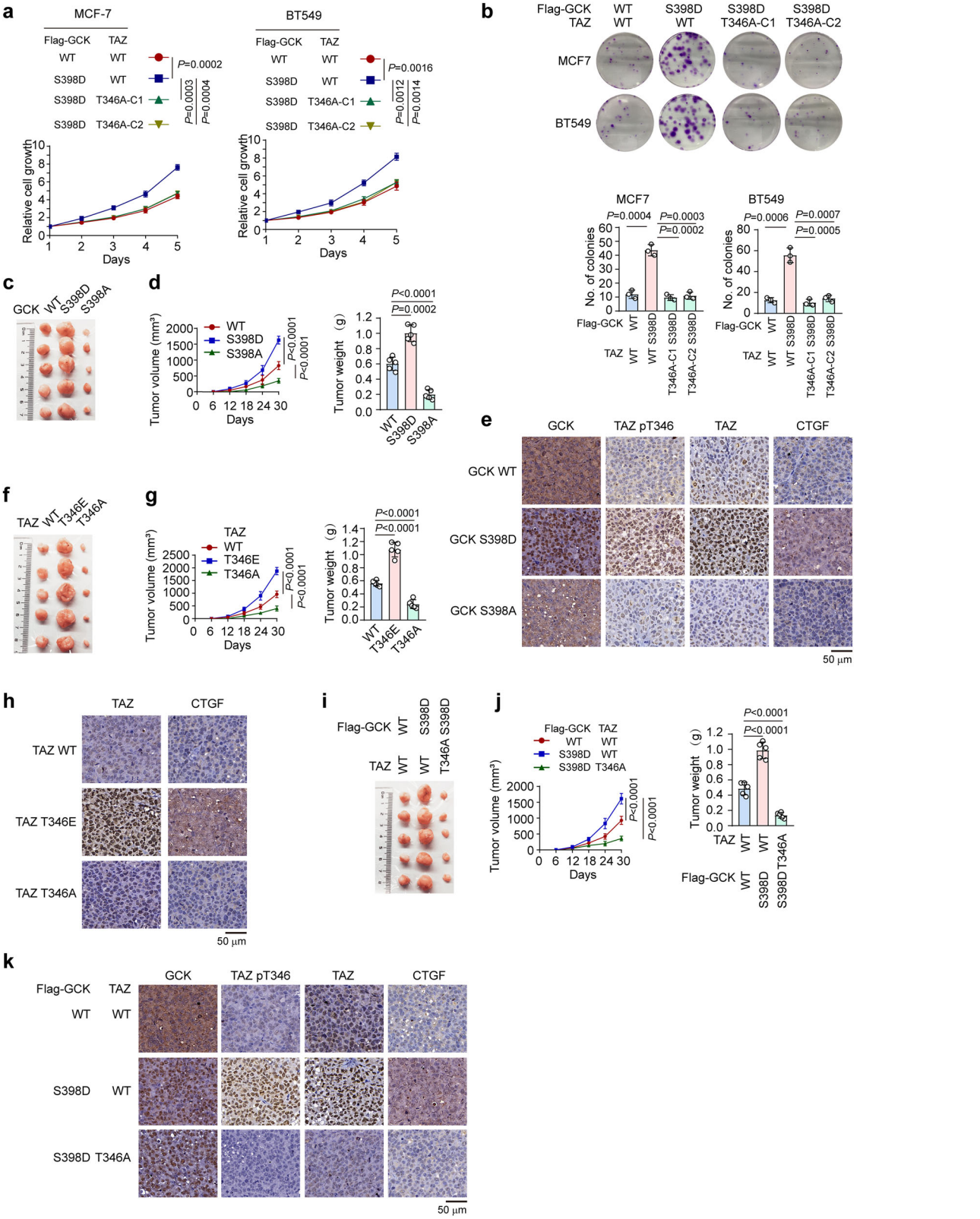

TAZ activation via Hippo-dependent or Hippo-independent regulation in response to cytokines, growth factors, oncogenic signals and changes in the growing environment has been intensively studied[14,32]. Elevated expression of genes associated with YAP/TAZ activity is correlated with high histological grade, enrichment of stem cell signatures, propensity for metastasis, and poor outcomes in patients with breast cancer[33,34]. In addition, TAZ nuclear staining is significantly enriched in high-grade breast tumour and serves as a predictor of poor clinical outcomes, underscoring the pivotal role of TAZ activation in breast cancer progression[33,35,36]. We revealed that hypoxia induces TAZ activation in tumour cells through nuclear GCK- and PIN1-mediated stabilization, a mechanism distinct from canonical Hippo pathway-mediated TAZ activation. Given that PIN1 is overexpressed in many types of cancers, including breast cancer[37], PIN1-mediated *cis-trans*

Fig. 5 | Nuclear GCK-mediated TAZ phosphorylation and activation promotes tumour cell proliferation and tumour growth. a Proliferation of MCF7 and BT549 cells with knocked-in expression of TAZ T346A and the indicated proteins was examined. The data are presented as the means ± SD, n = 3 independent experiments, two-tailed Student's t test. **b** Parental MCF7 and BT549 cells and the indicated clones with knock-in expression of TAZ T346A were transfected with the indicated plasmids. The colony formation ability of the MCF7 and BT549 cells was assessed. The data are presented as the means ± SD, n = 3 independent experiments, two-tailed Student's *t* test. **c**, **d** The parental MCF7 cells and the indicated clones with knock-in expression of GCK S398D or GCK S398A mutants were orthotopically injected into the fourth mammary fat pad of female BALB/c nude mice. The mice were sacrificed 30 days after cell injection. Tumour volume was calculated (n = 5 mice per group). Tumour weights were calculated (n = 5 mice per group). The data are presented as the means ± SDs; two-tailed Student's *t* test. **e** IHC analyses of mouse mammary tumours were performed with the indicated antibodies. Representative staining images are shown. **f**, **g** The parental MCF7 cells and the indicated clones with knock-in expression of TAZ T346E or TAZ T346A mutants were orthotopically injected into the fourth mammary fat pad of female BALB/c nude mice. The mice were sacrificed 30 days after cell injection. Tumour volume was calculated (n = 5 mice per group). Tumour weights were calculated (n = 5 mice per group). The data are presented as the means ± SDs; two-tailed Student's *t* test. **h** IHC analyses of mouse mammary tumours were performed with the indicated antibodies. Representative staining images are shown. **i**, **j** Parental MCF7 cells and the indicated clones with knock-in expression of TAZ T346A mutants were transfected with WT GCK or GCK S398D and orthotopically injected into the fourth mammary fat pad of female BALB/c nude mice. The mice were sacrificed 30 days after cell injection. The tumour volume was calculated (n = 5 mice per group). Tumour weights were calculated (n = 5 mice per group). The data are presented as the means ± SDs; one-way ANOVA. **k** IHC analyses of mouse mammary tumours were performed with the indicated antibodies. Representative staining images are shown. Source data are provided as a Source Data file.

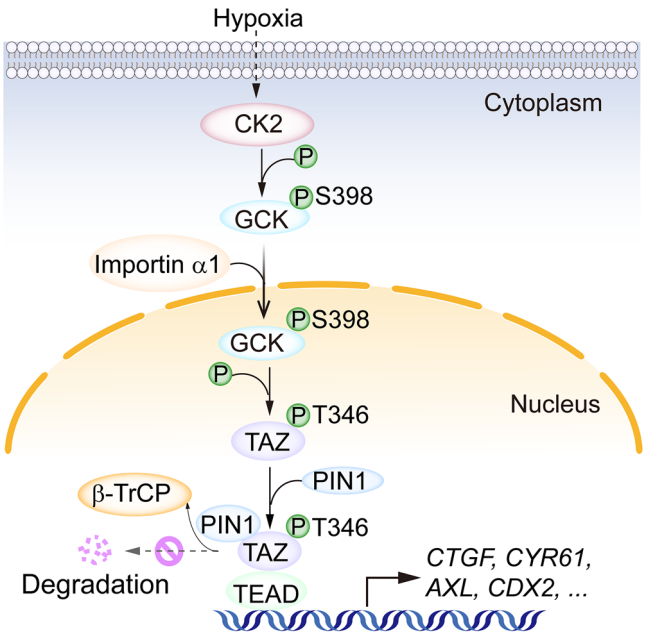

Fig. 6 | A schematic model showing that nucleus-translocated GCK acts as a protein kinase and phosphorylates TAZ to promote TAZ-TEAD transcriptional activity and tumour growth.

isomerization of GCK-phosphorylated TAZ highlights coordinated modifications of nuclear TAZ that leads to conformational changes and transcriptional activation of TAZ-TEAD. It has been shown that metabolic enzymes possess moonlighting functions, governing various essential cellular activities in tumour cells[1,6,38]. The finding that GCK acts as a protein kinase to phosphorylate TAZ in support of tumour growth underscores the potential of targeting GCK protein kinase for cancer treatment.

Methods

This work complies with all relevant ethical regulations. All animal experiments were approved by Ethics Committee Medical College of Qingdao University, including the Institutional Review Board and Institutional Animal Care and Use Committee.

Materials

Normal mouse IgG (sc-2025), normal rabbit IgG (sc-2027), GST (sc-138), Importin α1 (sc-55538), c-SRC (sc-8056), CK2α (sc373894), PIN1 (sc-46660), TAZ (sc-518026), CTGF (sc-101586) and protein A/G agarose (sc-2003) were obtained from Santa Cruz Biotechnology. ATP-γ-S (ab138911), p-nitrobenzyl mesylate (PNBM) (ab138910), GCK (ab88056), Lamin B1 (ab16048), HK2 (ab209847), CK2α pT360/S362 (ab119410) were purchased from Abcam. The ERK1/2 (#4695), ERK1/2 pT202/pY204 (#4370), AKT(#4685), AKT pS473 (#4060), c-Jun (#9165), c-Jun pS73 (#9164), c-SRC pY416 (#2101), Acetyl-CoA Carboxylase (ACC) (#3676S), ACC pS79 (#11818S), MAPK/APK2 (#3042), MAPKAPK-2 pT222 (#3316S), HRP-conjugated goat anti-mouse (#7076) and anti-rabbit (#7074) secondary antibodies were purchased from Cell Signaling Technology. Antibodies against β-actin (GB11001) were purchased from Servicebio. Rabbit polyclonal antibodies recognizing Ki67 (AB9260), anti-Flag (F3165), anti-HA (H9658), anti-Flag M2 agarose beads (A2220), anti-HA agarose beads (A2095), puromycin (P8833), streptavidin beads (S1638), EDTA-free protease inhibitor cocktail, dimethyl sulfoxide (DMSO), TBB, ATP, Tween 80, Dulbecco's modified Eagle's medium (DMEM), RPMI-1640, fetal bovine serum (FBS), and polyethylene glycol (PEG-400) were purchased from Sigma-Aldrich. Antibodies against HK1 (A23524) were purchased from ABclonal. GCK pS398 blocking peptide (RESR-pS-EDV) and TAZ pT346 blocking peptide (GENAGQ-pT-PMNINP) were synthesized by ABclonal and Hua Biotechnology, respectively. Rabbit polyclonal antibodies against GCK pS398 and TAZ pT346 were generated by Signalway Biotechnology. MK-2206 (S1078), SP600125 (S1460), U0126 (S1102), ivermectin (S1351) and reparixin (S8640) were purchased from Selleck Chemicals (USA). Hygromycin (HY-BO490), MG132 (HY-13259) and CHX (HY-12320) were purchased from MedChemExpress (Shanghai, China). GCK (19666-1-AP), TAZ (23306-1-AP), His-tag (66005-1-Ig), Flag-tag (20543-1-AP), HIF-1α (20960-1-AP) and α-Tubulin (66031-1-Ig) were purchased from Proteintech. DAPI, Alexa Fluor 488 goat anti-rabbit (A11008), Alexa Fluor 488 goat anti-mouse (A11001) and Alexa Fluor 594 goat anti-mouse (A11005); CIP (calf intestinal alkaline phosphatase) (18009019) and Lipofectamine 2000 (L3000015) transfection reagent were purchased from Thermo Fisher Scientific. Ni-NTA agarose was obtained from Qiagen. Glutathione sepharose (17-0756-05) and polyvinylidene difluoride (PVDF) membranes (Hybond-P) were obtained from GE Healthcare Life Sciences (USA). A nuclear/cytosol fractionation kit (K266-100) was obtained from BioVision. A dual luciferase reporter assay kit was purchased from Promega (72050). PolyJet transfection reagents were obtained from SignaGen.

Cell lines, cell culture conditions and drug treatment

The human breast cancer cell lines MCF7, BT549, BT-474, SK-BR-3 and human embryonic kidney cells (HEK293T) were obtained from ATCC. MCF7, BT549, BT-474, SK-BR-3 and HEK293T cells were maintained in DMEM (HyClone) supplemented with 10% fetal bovine serum (FBS). Viral infection was performed as previously described[39]. In all experiments, cells in the log phase were seeded, allowed to attach for 24 hours, and then the medium was replaced with fresh medium with or without the indicated drugs. For hypoxia treatment, cells were incubated in a Ruskinn InvivO2 workstation and oxygen tension was set to 1%.

Real-time PCR
Total RNA isolation, reverse transcription (RT), and real-time PCR were conducted as described previously[27]. Briefly, total RNA was extracted with TRIzol (Thermo Fisher Scientific) and reverse transcribed with Maxima Reverse Transcriptase (Thermo Fisher Scientific). Real-time PCR was performed with corresponding primers on a CFX Connect Real-Time PCR Detection System (Bio-Rad). The results were normalized to *ACTB* mRNA. The relative expression levels of the target genes were determined using the $2^{-\Delta CCt}$ method. The sequences of the PCR primers used for the amplification of genes are listed in Supplementary Data 1.

DNA constructs and mutagenesis
PCR-amplified human GCK, CK2, Erk2, TAZ, KPNA1-7, PIN1, and β-TrCP were cloned and inserted into the pcDNA3.1 (+)-hygromycin, pCDH-puromycin, pColdI, or pGEX-4T-1 vectors. All of the point mutations were generated by using the QuikChange site-directed mutagenesis kit (Stratagene, La Jolla, CA). shRNA was constructed via ligation of an oligonucleotide into an AgeI/EcoRI-digested pLKO.1 vector. The sgRNA was constructed via the ligation of an oligonucleotide into a BsmBI-digested lentiCRISPRv2 (Addgene, 52961) or a BbsI-digested PX458 vector. The pGL3-Basic-CTGF plasmid was constructed via the insertion of a PCR-amplified human CTGF promoter into a pGL3-Basic luciferase reporter vector via digestion with the KpnI and HindIII restriction enzymes. The sequences of the sgRNAs and shRNAs used are listed in Supplementary Data 1.

Lentivirus production and infection
Lentiviral packaging and infection were performed as previously described[39]. Briefly, HEK293T cells were cotransfected with pCDH, pLEX, Lenti-vector or pLKO.1 constructs and the packaging plasmids psPAX2 and pMD2.G. All media were removed after 6-8 hours and replaced with fresh DMEM + 10% FBS. The viruses were collected and filtered through a 0.45 μm membrane (Merck Millipore, GER) 48 hours after fresh media replacement. Virally infected cells were selected with puromycin for 96 hours.

Cell proliferation assay
For the cell proliferation assay, 800 MCF7 or BT549 cells were seeded in 96-well plates (Nest), and the viability of the cells was measured at the indicated time points. At the specified time points (Days 1-5), 10 μL of CCK8 (Promega) solution was added to each well. The cells were incubated at 37 °C for 1 hour. Then, the absorbance was measured in single-wavelength mode (at 450 nm) using a microplate reader (Thermo Fisher Scientific).

Transwell migration assay
For cell migration, 1×10^5 cells were seeded on Transwell filters with 8 mm pores in a 24-well plate chamber insert (Corning, USA) coated with Matrigel (Corning, USA) and DMEM (Matrigel:DMEM = 1:8)[40]. The top of the insert was filled with serum-free medium, while the bottom was filled with DMEM supplemented with 10% FBS. The cells were incubated for 24 hours and then fixed with 4% paraformaldehyde for 15 min. After washing with PBS, the cells at the top of the insert were scraped with a cotton swab. Cells adhering to the bottom were stained with hematoxylin for 1 min and then washed with double-distilled H_2O three times. The positively stained cells on the underside of the filters were photographed and examined under a microscope.

Subcellular fractionation
Cells at 60% confluence in 10 cm dishes were treated with or without hypoxia or the indicated drugs for the indicated times. Nuclear and cytosolic fractions were isolated from the cells using a nuclear/cytoplasmic fractionation kit[25].

GST pull-down assay
GST pulldown assays were performed as previously described[41]. Briefly, glutathione agarose beads were incubated with purified proteins overnight. The beads were then washed with lysis buffer five times.

Immunoprecipitation and immunoblotting analysis
Cells were lysed with lysis buffer (20 mM Tris-HCl [pH 7.5], 150 mM NaCl, 1 mM EDTA, 1 mM EGTA, and 1% Triton X-100) supplemented with protease inhibitor cocktails and PhosSTOP phosphatase inhibitor cocktails (Roche), and the supernatants were then incubated with the indicated antibodies and protein A/G agarose. The plates were incubated at 4 °C for 6 hours and then washed 4 times. Proteins were separated by SDS-PAGE and transferred to PVDF membranes. After blocking, the membranes were probed with various primary antibodies and then HRP-linked secondary antibodies. Signals were detected using the ECL method[42].

Purification of recombinant proteins
WT and mutant proteins were expressed in bacteria and purified as described previously[43]. Briefly, the corresponding constructs were expressed in the BL21 bacterial strain. The bacteria were cultured at 37 °C until the OD reached 0.6. Protein expression was induced with 0.1 mM IPTG for 18 hours at 16 °C. For GST-tagged proteins, cleared lysates were loaded onto a GSTrap HP column, washed with 5 column volumes of PBS, and subsequently eluted with 10 mM reduced glutathione. For His-tagged proteins, cleared lysates were loaded onto a Ni-NTA column, washed with 5 column volumes of 10 mM imidazole, and subsequently eluted with 250 mM imidazole. Proteins were then desalted by washing with PBS using 10 kDa cut-through spin columns.

Measurements of glucose consumption and lactate production
Cells were seeded in culture dishes, and the medium was changed after 6 h with non-serum DMEM. Cells were incubated for 24 h, and the culture medium was then collected for measurement of glucose and lactate concentrations. Glucose levels were determined by using a glucose assay kit (Beijing Boxbio Science & Technology Co., Ltd.). Lactate levels were determined by using a lactate assay kit (Nanjing Jiancheng Bioengineering Institute). All results were normalized to the final cell number.

Luciferase reporter assay
TAZ-TEAD activity was measured by a luciferase assay system as previously described[44]. Cells were cotransfected with TAZ-TEAD activity reporter luciferase plasmids (0.5 μg), the pRL-TK vector (as an internal control that contains Renilla luciferase sequences) (5 ng), and other plasmids (0.5 μg) by Lipofectamine 3000 (Thermo Fisher Scientific). Firefly and Renilla luciferase activities were measured using the dual-luciferase reporter assay, and the ratio of firefly/Renilla luciferase activity was determined.

In vitro kinase assay
The kinase reactions were performed as described previously[45]. In brief, bacterially purified recombinant His-GCK or His-TAZ (500 ng) was incubated with GST-CK2α or GST-GCK S398D (200 ng) in 30 μl of kinase buffer (25 mM Tris-HCl [pH 7.5], 5 mM beta-glycerophosphate, 2 mM dithiothreitol [DTT], 0.1 mM Na_3VO_4, and 10 mM $MgCl_2$) and then incubated with 10 mM ATP-γ-S at 30 °C for 1 h. The samples were alkylated with 50 mM PNBM/5% DMSO, incubated for 1 h at room temperature, and then subjected to SDS-PAGE and immunoblotting. An anti-thiophosphate ester antibody was used to detect the phosphorylated proteins.

In vitro isomerization assay
The isomerization rate was shown with the cis-peptide content, which was determined by isomer-specific proteolysis. Cis-peptides were

prepared by incubating the peptides with α-chymotrypsin at 0 °C for 2 min to completely hydrolyse the trans isomer at the 4-nitroanilide bond to obtain the pure cis-peptides. The pure cis-peptides were left to re-equilibrate. As the isomerization proceeded, aliquots were taken at the indicated time. Chymostatin was added to inactivate chymotrypsin. The absorbance of the released 4-nitroaniline was measured at 405 nm[10].

MD simulations

The structure of the human GCK was predicted by AlphaFold2 (https://alphafold.ebi.ac.uk/). The phosphorylated- GCK (pS398) was modelled with PyMOL (Version 2.1). The GCK structures were then minimized and refined using molecular dynamics simulations performed with the Amber 16 package (http://ambermd.org/) as previously described (Xu et al., 2022). The protein was solvated in a truncated octahedral TIP3P water box containing 109875 water molecules and was neutralized by Na+ using ff14SB force field (Maier et al., 2015). The system was first minimized with 5,000 steps of steepest descent and then 5,000 steps of conjugate gradient with the solute confined to their position by a harmonic force of 5 kcal/mol·Å2. A second minimization was then performed with all position restraints withdrawn. The system was then gradually heated from 0 to 310 K in the NVT ensemble over 100 ps with the solute confined to its position using a 3 kcal/mol·Å2 harmonic force potential. MD simulations were then performed in the NPT ensemble, and the position restraints were gradually removed within 100 ps. The production runs were conducted with a 200 ns simulation time and the pressure coupling set at 1 atm and a constant temperature of 310 K. The MD simulations used a time step of 2 fs, and all bonds involving hydrogen atoms were maintained at their standard lengths using the SHAKE algorithm. The particle-mesh Ewald (PME) method was used to model long-range electrostatic interactions. The molecules were drawn using PyMOL.

Immunofluorescence analysis

Immunofluorescence analyses were performed as described previously[46]. Briefly, cells grown on glass coverslips were washed with cold PBS and fixed with 4% paraformaldehyde for 15 min. The cells were then permeabilized with 0.25% Triton X-100 for 10 min. After blocking with 5% BSA for 1 h, the cells were probed with the indicated antibodies overnight at 4 °C. After washing, secondary antibodies with specific fluorescence dyes were added, and the cells were incubated for 1 h at room temperature. After being washed with PBS, the coverslips were mounted on glass slides with ProLong Gold Antifade Reagent and DAPI (Thermo Fisher Scientific). Images were taken with a Zeiss LSM 900 confocal microscope.

Genomic editing

Genomic mutations in MCF7 and BT549 cells were generated using CRISPR-Cas9 genome-editing technology as described previously[47]. Single-guide RNAs (sgRNAs) were designed to target the genomic areas adjacent to human and mouse GCK or WWTR1 mutation sites using the CRISPR design tool (https://www.benchling.com/). The annealed guide oligos containing overhangs were inserted into the PX458 vector (Addgene) digested by the BbsI restriction enzyme. In a 24-well plate, cells at 60% confluence were cotransfected with a single-stranded donor oligonucleotide (ssODN) (20 pmol) used as a template to introduce mutations and a vector (0.5 mg) able to coexpress a sgRNA targeting the human or mouse GCK or WWTR1 gene and a wild-type hSpCas9 tagged with puromycin. Twenty-four hours after transfection, the cells were treated with puromycin for 48 h, and puromycin-positive cells were seeded in 96-well plates. Genotyping was performed by sequencing PCR products amplified from primers spanning the mutation area. The ssOND sequences and primers used for sgRNA cloning and genomic DNA sequencing are listed in Supplementary Data 1.

Mass spectrometry analysis

To identify nuclear GCK-interacting proteins, we expressed Flag-GCK S398D in MCF7 cells under normoxic or hypoxic conditions (8 h treatment). Cell lysates were immunoprecipitated using anti-Flag antibody, separated by SDS-PAGE, and visualized by Coomassie blue staining. Distinct protein bands were excised and subjected to in-gel digestion with 200 ng sequencing-grade trypsin (Promega) in 50 mM ammonium bicarbonate buffer containing RapiGest (Waters) at 37 °C overnight. Digested peptides were analyzed by LC-MS/MS using an Orbitrap Elite mass spectrometer (Thermo Fisher Scientific). Protein identification was performed using Proteome Discoverer (v1.4) with Mascot search engine (v2.3) against the UniProt database.

For TAZ phosphorylation site identification, we performed in vitro kinase assays as previously described[8].

Phosphorylated TAZ was digested overnight at 37 °C with 200 ng mass spectrometry-grade trypsin in 50 mM Tris-HCl (pH 8.0) containing 0.5 mM zinc acetate. LC-MS/MS analysis (Orbitrap Elite) identified a + 5 charged tryptic fragment (m/z 5201.28923 Da) corresponding to TAZ residues 309-356 (EQSTDSGLGLGCYSVPTTPEDFLSNVDEMDTGENAGQTPMNINPQQTR) (XCorr = 7.02), confirming phosphorylation at Thr346.

Animal studies

Five-week-old female athymic BALB/c nude mice were housed under specific pathogen-free conditions in a 14 h light/10 h dark cycle. Ambient temperature (21-23 °C, 50% humidity) with access to water and food ad libitum. The animals were acclimated for 1 week before the experiments. One million MCF7 cells or MCF7 cells reconstituted by different GCK or TAZ mutants were collected in 20 µl Dulbecco's modified Eagle medium with 50% Matrigel, was orthotopically injected into the fourth mammary fat pads of female BALB/c mice (5 mice per group). Tumour volume was measured with a caliper every 6 days and calculated using length a and width b: $V = ab^2/2$. Thirty days after injection, the primary tumours of the mice were harvested, fixed in 4% formaldehyde, and embedded in paraffin. Tumour formation and phenotype were determined by further molecular and pathological analyses, including H&E and IHC staining[48].

The maximal tumour size permitted by ethics committee is 2000 mm^3, and the maximal tumour size did not exceed the limit. Animal experiments were conducted following the National Institutes of Health guidelines and were approved by the Ethics Committee Medical College of Qingdao University.

Hematoxylin and eosin (H&E) and immunohistochemistry (IHC) analyses

H&E and IHC staining were performed as previously described[49]. Briefly, the mice were sacrificed, and the primary tumour and lung tissues were collected, the lung tissues were inflated, and then the tissues were fixed in 10% formalin, embedded in paraffin, and sectioned at 5 µm, followed by staining with hematoxylin and eosin (H&E).

For IHC staining, the slides were deparaffinized in xylene and ethanol and rehydrated in water. Antigen retrieval was performed by heating the slides in a microwave for 20 minutes in sodium citrate buffer (pH 6.0). The slides were quenched in hydrogen peroxide (3%) to block endogenous peroxidase activity and then washed in PBS. The membranes were incubated with primary antibodies at 4 °C overnight, after which the Vectastain ABC kit (Vector Laboratories) was used to visualize the staining according to the manufacturer's instructions.

Statistics and reproducibility

Statistical analysis was performed using GraphPad Prism 8 (GraphPad Software Inc., San Diego, CA, USA). Unless indicated, data were analyzed by two-tailed Student's t tests for two groups. One-way ANOVA followed by the Newman-Keuls multiple comparison test was used to analyze the statistical significance among multiple groups. Survival

analysis was performed using the Kaplan-Meier method, and data were compared by the log-rank (Mantel-Cox) test. The data are shown as the mean ± SD. A P value <0.05 was considered to indicate statistical significance. All immunoblotting analyses were independently repeated three times, yielding similar results.

Reporting summary

Further information on research design is available in the Nature Portfolio Reporting Summary linked to this article.

Data availability

The mass spectrometry proteomics data generated in this study have been deposited publicly to the ProteomeXchange Consortium via the PRIDE partner repository with dataset identifier PXD061668. The remaining data are available within the Article, Supplementary Information or Source Data file. Source data are provided with this paper.

References

1. Li, X., Egervari, G., Wang, Y., Berger, S. L. & Lu, Z. Regulation of chromatin and gene expression by metabolic enzymes and metabolites. *Nat. Rev. Mol. Cell Biol.* **19**, 563–578 (2018).
2. Guo, D., Meng, Y., Jiang, X. & Lu, Z. Hexokinases in cancer and other pathologies. *Cell Insight* **2**, 100077 (2023).
3. Lu, B., Munoz-Gomez, M. & Ikeda, Y. The two major glucokinase isoforms show conserved functionality in beta-cells despite different subcellular distribution. *Biol. Chem.* **399**, 565–576 (2018).
4. Bian, X. et al. Regulation of gene expression by glycolytic and gluconeogenic enzymes. *Trends Cell Biol.* **32**, 786–799 (2022).
5. Li, X. et al. Mitochondria-translocated PGK1 functions as a protein kinase to coordinate glycolysis and the TCA cycle in tumorigenesis. *Mol. Cell* **61**, 705–719 (2016).
6. Xu, D. et al. The evolving landscape of noncanonical functions of metabolic enzymes in cancer and other pathologies. *Cell Metab.* **33**, 33–50 (2021).
7. Guo, D. et al. Aerobic glycolysis promotes tumor immune evasion by hexokinase2-mediated phosphorylation of IkappaBalpha. *Cell Metab.* **34**, 1312–1324.e1316 (2022).
8. Yang, W. et al. PKM2 phosphorylates histone H3 and promotes gene transcription and tumorigenesis. *Cell* **150**, 685–696 (2012).
9. Yang, W. et al. Nuclear PKM2 regulates beta-catenin transactivation upon EGFR activation. *Nature* **480**, 118–122 (2011).
10. Yang, W. et al. ERK1/2-dependent phosphorylation and nuclear translocation of PKM2 promotes the Warburg effect. *Nat. Cell Biol.* **14**, 1295–1304 (2012).
11. Yang, W. et al. EGFR-induced and PKCepsilon monoubiquitylation-dependent NF-kappaB activation upregulates PKM2 expression and promotes tumorigenesis. *Mol. Cell* **48**, 771–784 (2012).
12. Yang, W. & Lu, Z. Pyruvate kinase M2 at a glance. *J. Cell Sci.* **128**, 1655–1660 (2015).
13. Pfleger, C. M. The hippo pathway: a master regulatory network important in development and dysregulated in disease. *Curr. Top. Dev. Biol.* **123**, 181–228 (2017).
14. Yu, F. X., Zhao, B. & Guan, K. L. Hippo pathway in organ size control, tissue homeostasis, and cancer. *Cell* **163**, 811–828 (2015).
15. Zanconato, F., Cordenonsi, M. & Piccolo, S. YAP/TAZ at the roots of cancer. *Cancer Cell* **29**, 783–803 (2016).
16. Harvey, K. F., Pfleger, C. M. & Hariharan, I. K. The Drosophila Mst ortholog, hippo, restricts growth and cell proliferation and promotes apoptosis. *Cell* **114**, 457–467 (2003).
17. Udan, R. S., Kango-Singh, M., Nolo, R., Tao, C. & Halder, G. Hippo promotes proliferation arrest and apoptosis in the Salvador/Warts pathway. *Nat. Cell Biol.* **5**, 914–920 (2003).
18. Wu, S., Huang, J., Dong, J. & Pan, D. hippo encodes a Ste-20 family protein kinase that restricts cell proliferation and promotes apoptosis in conjunction with salvador and warts. *Cell* **114**, 445–456 (2003).
19. Liu, C. Y. et al. The hippo tumor pathway promotes TAZ degradation by phosphorylating a phosphodegron and recruiting the SCFbeta-TrCP E3 ligase. *J. Biol. Chem.* **285**, 37159–37169 (2010).
20. Guo, X. et al. Single tumor-initiating cells evade immune clearance by recruiting type II macrophages. *Genes Dev.* **31**, 247–259 (2017).
21. Moroishi, T. et al. The hippo pathway kinases LATS1/2 suppress cancer immunity. *Cell* **167**, 1525–1539.e1517 (2016).
22. Wang, G. et al. Targeting YAP-dependent MDSC infiltration impairs tumor progression. *Cancer Discov.* **6**, 80–95 (2016).
23. Janse van Rensburg, H. J. et al. The hippo pathway component TAZ promotes immune evasion in human cancer through PD-L1. *Cancer Res.* **78**, 1457–1470 (2018).
24. Ji, H. et al. EGF-induced ERK activation promotes CK2-mediated disassociation of alpha-Catenin from beta-Catenin and transactivation of beta-Catenin. *Mol. Cell* **36**, 547–559 (2009).
25. Wang, Z. et al. Fructose-1,6-bisphosphatase 1 functions as a protein phosphatase to dephosphorylate histone H3 and suppresses PPARalpha-regulated gene transcription and tumour growth. *Nat. Cell Biol.* **24**, 1655–1665 (2022).
26. Lei, Q. Y. et al. TAZ promotes cell proliferation and epithelial-mesenchymal transition and is inhibited by the hippo pathway. *Mol. Cell. Biol.* **28**, 2426–2436 (2008).
27. Xu, D. et al. The gluconeogenic enzyme PCK1 phosphorylates INSIG1/2 for lipogenesis. *Nature* **580**, 530–535 (2020).
28. Liu, R. et al. Choline kinase alpha 2 acts as a protein kinase to promote lipolysis of lipid droplets. *Mol. Cell* **81**, 2722–2735.e2729 (2021).
29. Lu, Z. & Hunter, T. Prolyl isomerase Pin1 in cancer. *Cell Res.* **24**, 1033–1049 (2014).
30. Zhao, B. et al. TEAD mediates YAP-dependent gene induction and growth control. *Genes Dev.* **22**, 1962–1971 (2008).
31. Guo, D., Meng, Y., Zhao, G., Wu, Q. & Lu, Z. Moonlighting functions of glucose metabolic enzymes and metabolites in cancer. *Nat. Rev. Cancer* **25**, 426–446 (2025).
32. Zhang, Z. et al. OTUB2 promotes cancer metastasis via hippo-independent activation of YAP and TAZ. *Mol. Cell* **73**, 7–21.e27 (2019).
33. Cordenonsi, M. et al. The Hippo transducer TAZ confers cancer stem cell-related traits on breast cancer cells. *Cell* **147**, 759–772 (2011).
34. Zanconato, F. et al. Genome-wide association between YAP/TAZ/TEAD and AP-1 at enhancers drives oncogenic growth. *Nat. cell Biol.* **17**, 1218–1227 (2015).
35. Bartucci, M. et al. TAZ is required for metastatic activity and chemoresistance of breast cancer stem cells. *Oncogene* **34**, 681–690 (2015).
36. Diaz-Martin, J. et al. Nuclear TAZ expression associates with the triple-negative phenotype in breast cancer. *Endocr. Relat. Cancer* **22**, 443–454 (2015).
37. Caligiuri, I., Vincenzo, C., Asano, T., Kumar, V. & Rizzolio, F. The metabolic crosstalk between PIN1 and the tumour microenvironment. *Semin. Cancer Biol.* **91**, 143–157 (2023).
38. Lu, Z. & Hunter, T. Metabolic kinases moonlighting as protein kinases. *Trends Biochem. Sci.* **43**, 301–310 (2018).
39. Zhao, G. et al. Cullin5 deficiency promotes small-cell lung cancer metastasis by stabilizing integrin beta1. *J. Clin. Investig.* **129**, 972–987 (2019).
40. Zheng, Y., Yang, W., Aldape, K., He, J. & Lu, Z. Epidermal growth factor (EGF)-enhanced vascular cell adhesion molecule-1 (VCAM-1) expression promotes macrophage and glioblastoma cell interaction and tumor cell invasion. *J. Biol. Chem.* **288**, 31488–31495 (2013).
41. Li, M. et al. Fructose-1,6-bisphosphatase 1 dephosphorylates and inhibits TERT for tumor suppression. *Nat. Chem. Biol.* **20**, 1505–1513 (2024).
42. Li, X. et al. Nuclear PGK1 alleviates ADP-dependent inhibition of CDC7 to promote DNA replication. *Mol. Cell* **72**, 650–660.e8 (2018).

43. Xu, D. et al. The protein kinase activity of fructokinase A specifies the antioxidant responses of tumor cells by phosphorylating p62. *Sci. Adv.* **5**, eaav4570 (2019).
44. Qian, X. et al. KDM3A senses oxygen availability to regulate PGC-1alpha-mediated mitochondrial biogenesis. *Mol. Cell* **76**, 885–895.e887 (2019).
45. Qian, X. et al. Conversion of PRPS hexamer to monomer by AMPK-mediated phosphorylation inhibits nucleotide synthesis in response to energy stress. *Cancer Discov.* **8**, 94–107 (2018).
46. Zheng, Y. et al. Secreted and O-GlcNAcylated MIF binds to the human EGF receptor and inhibits its activation. *Nat. Cell Biol.* **17**, 1348–1355 (2015).
47. Li, X. et al. Programmable base editing of mutated TERT promoter inhibits brain tumour growth. *Nat. Cell Biol.* **22**, 282–288 (2020).
48. Wu, K. et al. Creatine kinase B suppresses ferroptosis by phosphorylating GPX4 through a moonlighting function. *Nat. Cell Biol.* **25**, 714–725 (2023).
49. Ma, Q. et al. The moonlighting function of glycolytic enzyme enolase-1 promotes choline phospholipid metabolism and tumor cell proliferation. *Proc. Natl. Acad. Sci. USA* **120**, e2209435120 (2023).

Acknowledgements

This study was supported by grants from the National Natural Science Foundation of China (82188102, 82030074, Z.L.; 82073061, J.F.; 82002445, G.Z.; 82372816, D.G.), the Ministry of Science and Technology of the People's Republic of China (2020YFA0803300, Z.L., J.F.), and the National Center of Technology Innovation for Biopharmaceuticals (NCTIB2022HS02006, Z.L.). Z.L. is the Kuancheng Wang Distinguished Chair.

Author contributions

Z.L. conceived the study; Z.L. and G.Z. designed the study; G.Z., S.L., H.Z., Q.M., H.J., Q.X., L.W., Juanjuan Liu, Jie Lun, D.G., R.W., R.X., Y.D., L.M., W.Q., and J.F. performed the experiments and analyzed the data; J.F. and W.Q. reviewed and edited the manuscript; Z.L. and G.Z. wrote the paper with comments from all of the authors.

Competing interests

Z.L. owns shares in Signalway Biotechnology (Pearland, TX), which supplied the rabbit antibodies that recognize GCK pS398 and TAZ pT346. Z.L.'s interest in this company had no bearing on its being chosen to supply these reagents. The remaining authors declare no competing interests.

Additional information

Supplementary information The online version contains supplementary material available at https://doi.org/10.1038/s41467-025-62566-4.

Correspondence and requests for materials should be addressed to Wensheng Qiu, Jing Fang or Zhimin Lu.

Peer review information *Nature Communications* thanks Loranne Agius and the other anonymous reviewer(s) for their contribution to the peer review of this work. A peer review file is available.